Cement and Concrete Research 39 (2009) 825–831

Contents lists available at ScienceDirect

Cement and Concrete Research

journal homepage: http://ees.elsevier.com/CEMCON/default.asp

Real-time evolution of electrical resistance in cracking concrete

C. Boulay *, S. Dal Pont, P. Belin

Laboratoire Central des Ponts et Chaussées, Division Bétons et Composites Cimentaires, LCPC-BCC, Université Paris-Est, 58 bd Lefebvre, 75732 Paris cedex 15, France

ARTICLE INFO

Article history:
Received 29 January 2009
Accepted 1 June 2009

Keywords:
Splitting test
Concrete electrical resistance
Traversing crack
Conductance-cracked concrete real-time relation

ABSTRACT

The aim of this paper is to present a real-time relation between the evolution of the electrical resistance and the crack width opening in a saturated concrete sample. The splitting (Brazilian) test has been enhanced and adapted so that the monitoring of a single crack opening and the electrical resistance of the specimen are possible. The experimental results showed that the electrical resistance is constant before the peak (when no crack is observed) and decreases only when the peak of load is reached and when a crack is initiated. No threshold value and no delay between the crack opening and the resistance evolution have been observed, even in the case of a breathing crack. The evolution of the electrical conductance has then been modeled by taking into account the (simplified) morphology of the crack and assuming a constant value for the electrolyte conductivity. The model and the experimental conductance through a traversing crack have proved to be in good agreement.

1. Introduction

A satisfying description of the microstructure of a heterogeneous material such as concrete should take into account both porosity and cracks (micro-cracks provoked by internal stresses due to autogenous shrinkage restrained by the aggregates [1] as well as cracks due to external loadings). Indeed, their inevitable presence weakens the porous matrix resistance and constitutes a preferential flow path for fluids, gas and pollutants [2]: material durability is therefore seriously affected. A proper numerical modeling of concrete subjected to severe loading conditions should take into account these phenomena: the description of the behavior of a cracked concrete studied as a multi-phase porous medium requires the definition of an experimental constitutive law relating the typical durability indicators (such as permeability, diffusivity, electrical resistivity, …) to the crack width.

This paper deals with the feasibility of transfer properties measurement tests during the post-peak cracking phase of concrete. Observations on pre-cracked concrete [3–5] evidenced a sharp increase of parameters such as chloride diffusivity or gas/water permeability. However, a proper description of the evolution of these properties should be monitored in real time as cracks open in the specimen. In such a way, parasite effects related to time (e.g. crack healing, external ambient conditions changes, crack breathing, …) or post-treatments (e.g. modifications of the hygrometric conditions of the sample) can be avoided. In this paper, attention is focused firstly on the mechanical test and the geometrical characterization of the cracks by means of a displacement measurement system.

Usually, mechanical tests used to explore the post-peak phase lead to distributed multiple crack patterns [3,6,7] or to single well-defined crack [4,5,8,9]. The former geometry is obviously more difficult to characterize than the latter. Given our objective, tests leading to a unique crack were chosen. Direct tensile test, bending test or Brazilian test are good candidates but, for the sake of simplicity and with the aim of performing original real-time transfer properties measurements during the loading, the Brazilian splitting test has been retained and enhanced. Moreover such a test leads to strong stress gradients though ensuring a less tortuous visible crack [10,11]. For the purpose of the feasibility test, the crack width has been limited to 0.1 mm. This threshold has been chosen to avoid multiple cracks generally observed when the opening of the crack becomes important. Moreover, a 100 μm width is sufficient for evaluating the existence of an eventual threshold effect and is comparable to the crack widths suggested when dealing with leakage problems in nuclear vessels or containment structures [12].

In the second part of the paper, a set-up measuring electrical resistance / conductivity of the cracked specimen will be presented. Electrical resistivity is usually considered as an indicator of concrete pore connectivity [13] and is commonly enumerated among the tools used for evaluating the performance of a structure in terms of service life [14,15]. Moreover, a relation exists between resistivity and chloride diffusion [16]. In this paper, a macroscopic-measurable quantity such as the electrical resistance of the system concrete specimen-ionic solution has been monitored in real time during concrete cracking. The experimental results showed that the electrical resistance is constant before the peak (when no crack is observed) and rapidly

* Corresponding author. Tel.: +33 1 40 43 52 96; fax: +33 1 40 43 54 98.
E-mail address: claude.boulay@lcpc.fr (C. Boulay).

0008-8846/$ – see front matter © 2009 Elsevier Ltd. All rights reserved.
doi:10.1016/j.cemconres.2009.06.003

Table 1
Mix design.

Components	Mass (kg/m^3)
Cement CEM I 52,5 N PMES CP2 Lafarge/Le Havre	340
Water	184.22
Sand(river): Bernières 0/4	739.45
Gravels(river): Bernières 6.3/20	1072.14

decreases only when the peak of load is reached and when a crack is initiated.

2. Mechanical testing conditions

The mix proportions of the concrete used for the design of the tests are given in Table 1.

Cylinders with 100 cm^2 in cross section and 22 cm in height were cast in steel molds for the sake of a good geometry, i.e. common non-steel moulds can lead to misshapen generatrixes. They were removed from the steel moulds at 24 h and cured wrapped in a self-adhesive aluminium tape and aged for more than three months at the time of the tests. Each cylinder was sliced in discs and each face was grounded to reach a thickness of 5 cm (three samples can be drawn from one cylinder). Splitting tests were performed on a $\pm$500 kN hydraulic press equipped with a feedback. The press not only performs the classical displacement/load controlled tests but also allows to compute mathematical (real time) combinations of measurements in order to create feedback signals to control the test.

During the tests, a lower bearing plate (Fig. 1, Ref. [1]) is fixed at the top end of the piston (bottom of the testing machine) while the upper bearing plate is a part of a ball socket joint (Ref. [2]) under the load cell (Ref. [3]). The sample (Ref. [4]) is loaded between these bearing plates. As permeation tests have to be performed, no displacement transducer can be fixed or glued on both ends of the specimen (as, e.g. in Ref. [8] or [4]). Displacements are then measured on each side of the horizontal diameter. As mentioned by Refs. [4] and [8], cracks generally open on one face and then propagate towards the other face. Hence, two pairs of LVDTs (stroke = $\pm$1 mm, Ref. [5]) were maintained by a rigid frame (Ref. [6]) (sustained by the lower plate of the press), in order to measure the variations of two diameters.

The distance between the axis of the LVDTs is 3 cm. The tips of the LVDTs are not directly in contact with the sample lateral surface but lie on glass blades (Ref. [7]) glued on each side (axial displacements of each LVDT and orthogonal displacements close to the tip of the transducers are of the same order of magnitude). The frame geometry can be influenced by temperature variations during the test so thermal displacements can affect the measurements. For this reason, the temperature of the frame is measured with a platinum probe. The thermal coefficient of the frame is 0.00317 mm/k.

Load distribution into the sample is usually obtained using plywood or cardboard [4,8,17]: nevertheless we observed that in such a case displacements were strongly not symmetric, even in the pre-peak (elastic) zone. The use of adhesive tape stripes replacing the plywood led to more symmetrical cracks.

Before loading, samples are aligned and maintained on the lower plate with a rig (Ref. [8]) avoiding any displacement during the docking phase (between the sample and the upper plate) while the ball socket joint rotates to counteract any eventual out of parallelism of the bearing lines. After docking, the lateral movement of the ball socket joint is restrained by the means of compliant spacers (Ref. [9]). The four measured displacements are named (Δl_{fl}, Δl_{fr}, Δl_{rl}, Δl_{rr}), respectively the front left displacement, the front right, the rear left and the rear right. The sum of the front displacements gives the variations of the diameter 15 mm in front of the mid section ($\Delta \varnothing_{fm} = \Delta l_{fl} + \Delta l_{fr}$) while the sum of the rear displacements gives the variations of the diameter 15 mm backward ($\Delta \varnothing_{rm} = \Delta l_{rl} + \Delta l_{rr}$). The mean value ($\varnothing$) of these two variations, calculated by the press in real time, becomes the press control variable.

Once the specimen is ready on the press, the testing protocol schedules a manual docking until a pre-load of about 0.5 kN. A

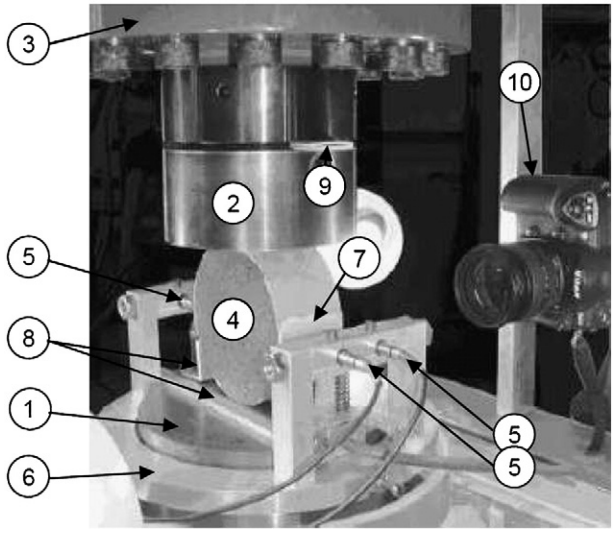

Fig. 1. Test settings.

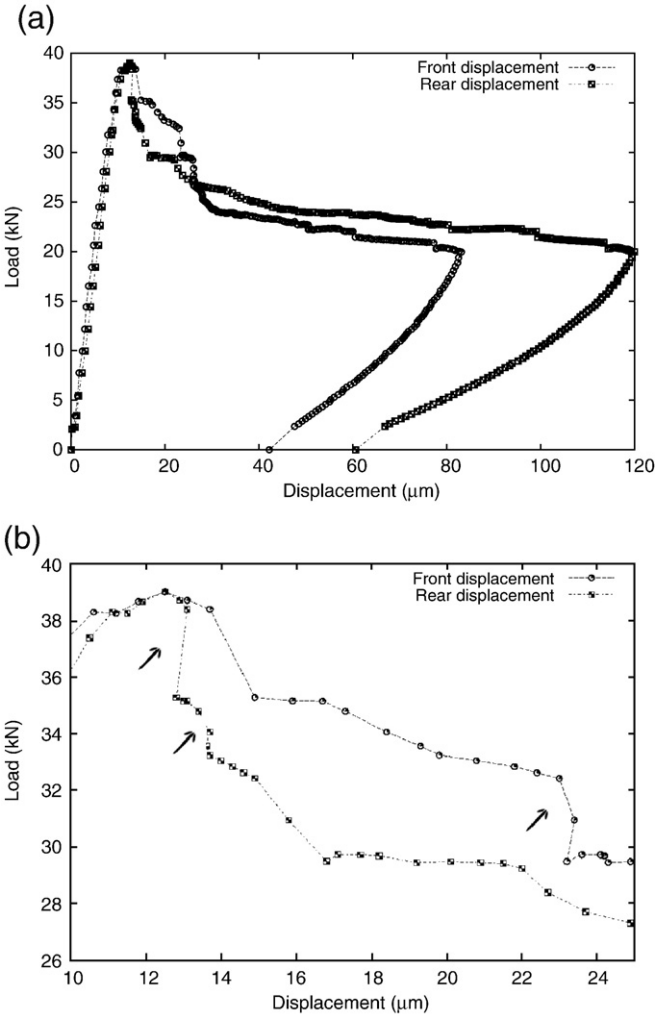

Fig. 2. LVDTs diameter variations.

displacement ramp is started at a rate of $\Delta\varnothing/dt = 10$ µm/min. When the mean displacement reaches a value of approximately 100 µm, the ramp is decreased to about 20 µm. Then a loading rate of 5 kN/min is applied back to 2 kN. Finally, the sample is completely unloaded with the control on the displacement of the piston.

3. Crack opening measuring system

3.1. Experimental analysis with displacement transducers (LVDT)

As pointed out in the previous section, the heterogeneity of concrete leads to an asymmetric behavior between the two faces: results are therefore given on both sides (rear and front) of the specimen. The analysis of diameter variations (on LVDTs) in the pre-peak zone (Fig. 2(a)) shows similar measurements on the front and rear. It confirms that the boundary conditions imposed on the specimen and presented in Section 2 are well adapted. Differences between rear and front measurements are shown in the post-peak period. It confirms the necessity of a control on the mean value of the displacements. A zoom (Fig. 2(b)) on this curve indicates (see arrows) that the displacement on one face snaps back while, on the other face, the displacement increases. A displacement control with only one measurement would have failed because of these quick recoveries.

The Crack Opening Displacement (COD) is calculated from measured displacements in two steps. In the first step, the diameter variations on each face of the sample (Fig. 3(a)) are calculated from the diameter variations in the axis of LVDTs $\Delta\varnothing_{fm}$, $\Delta\varnothing_{rm}$. For this purpose, it

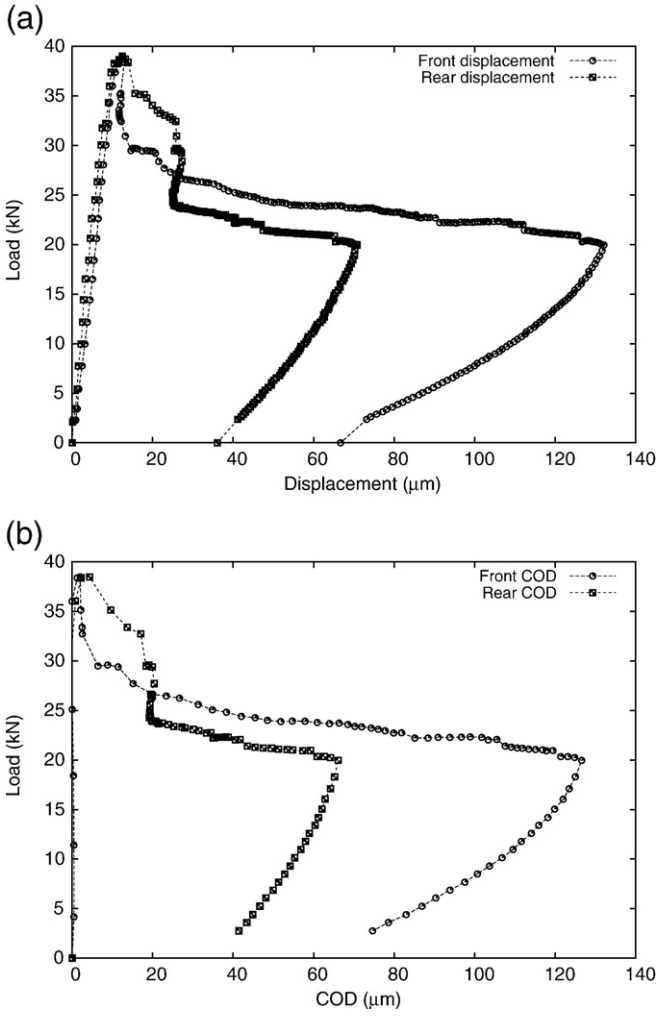

Fig. 3. Diameter variations on the faces of the sample and COD at mid height.

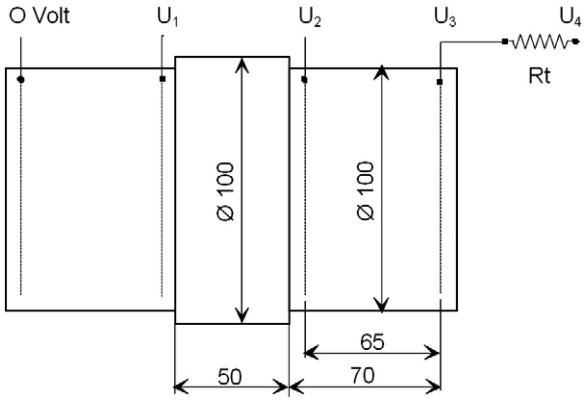

Fig. 4. Electrical scheme.

is supposed that plane sections remain plane. This calculation emphasizes the discrepancy between the rear and the front face after the peak. The second step consists in removing the elastic part of these variations provided that, after the peak, the sample is split into two elastic blocks without damaged zones on the lips of the crack. The elastic part is obtained via the pre-peak behavior (slope of the curve for the front face equals to 3.7 kN/µm and 3.77 kN/µm for the rear face).

In Fig. 3(b) a typical result is presented. One can observe that while the front COD increases just after the peak, the rear COD is nearly blocked. At about 19 µm for the front COD, the crack stops and snaps back while the rear COD starts to increase. This scenario, also observed on other samples, illustrates that this asymmetrical cracking process is not an exception but the rule and is related to the heterogeneous nature of the concrete. The crack propagates from one side to the other in the first few micrometers of COD. During further crack opening, frictions through the crack (between aggregates and matrix) are involved in the opening mechanisms. These frictions are attributed to both autogenous shrinkage of the cement paste restrained by the aggregates [1,18] and roughness itself of the aggregates. Depending on the place where the more important friction occurs, the movements involved in the crack opening process lead to snaps back on one side or the other. Snaps back occur as long as the lips of the crack are in contact [19]. This mechanism should be taken into account in numerical modeling, i.e. a full 3D analysis is preferable when dealing with cracking concrete. The crack area is also pertinent in numerical modeling but the LVDT measuring system cannot provide this kind of information. Such an information can be obtained via microscopy observations or via the Digital Image Correlation technique (DIC) (see for example Refs. [20–24]). However, these techniques are not compatible with the electrical resistance

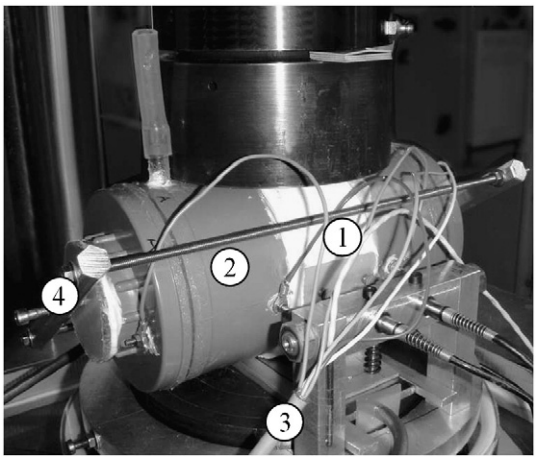

Fig. 5. Final configuration of the set-up. 1. Sample; 2. Vessels; 3. Wiring; 4. Clamping device.

measuring system (as the faces of the samples are covered) and have not been retained for measuring the crack width. It is planned in a forthcoming work to make use of the DIC to characterize the morphology of the crack by correlating via a statistical law the width and the height of the crack [24].

4. Electrical resistance measuring system

The electrical resistance of concrete is the parameter which is actually measured (during the mechanical loading) between electrodes placed on each side of the specimen. In the following we will also refer to resistivity and conductivity (the inverse of resistivity) as these parameters are often used in the literature concerning concrete durability [13–16,25,26], ... In saturated conditions and in sound concrete, as current passes through the specimen via the porous network, resistivity is usually considered as an indirect measurement of the concrete porosity and tortuosity. Resistivity can also be related to the chloride diffusion coefficient and is therefore considered as a durability indicator of concrete [13–16,26]. When dealing with cracked concrete (diffuse and/or single residual cracks), a sharp increase of liquid/gas permeability [4,6,8], chloride permeability [3,5,9], and electrical conductivity [13,25] has been observed.

The objective of this study is to describe, in real time, the electrical conductance evolution during concrete cracking in saturated conditions.

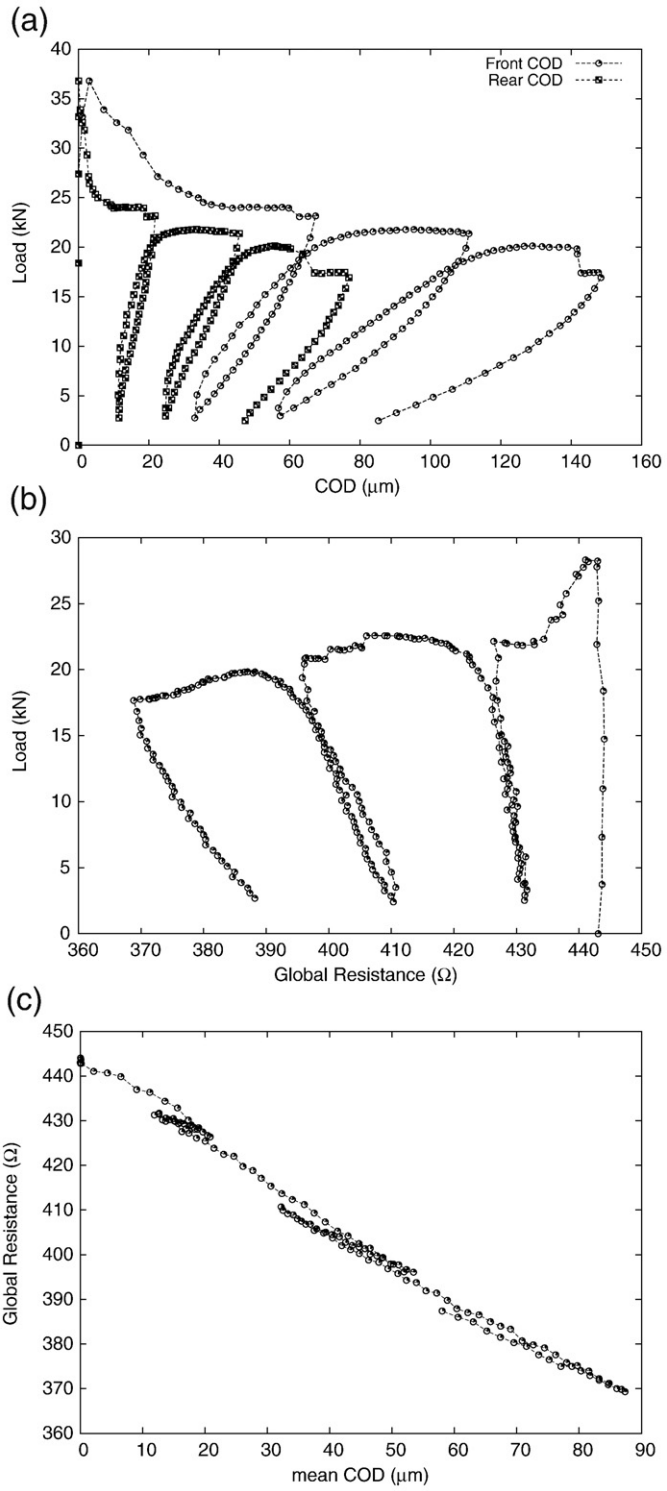

Fig. 6. Evolutions of the mean COD and the total resistance.

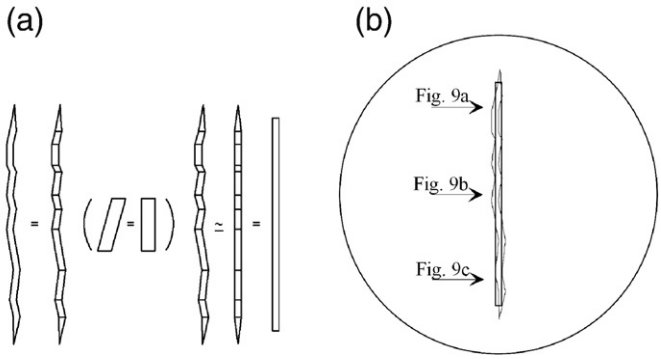

Fig. 7. Crack geometry modeling.

4.1. Preconditioning of the specimen

After sawing and grinding (see Section 2), the surfaces of the disc are dried and PVC containers (standard sewer pipes) are glued on it with silicon rubber. The titanium platinum-coated electrodes (grids) for voltage measurements are fixed in the containers. When silicon rubber is polymerized, specimens are placed in a vacuum container (1–5 kPa) for 4 h in order to remove the air from pores of concrete (i.e. create vacuum conditions). An insulating paint is applied on the specimen's diametric surface in order to avoid drying during the test. The container is then filled with an ionic solution (NaOH/6.01 g/l–KOH/8.94 g/l) so as to immerse completely the specimen for 48 ± 2 h. This solution is supposed to fill the pores and to be representative of the interstitial solution of the concrete [27]. During this phase, the

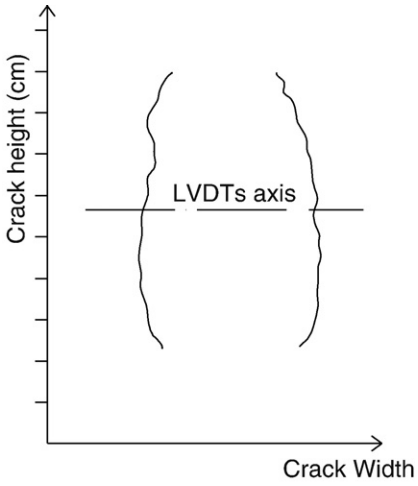

Fig. 8. DIC left/right crack lips on a loaded specimen (crack width ≈100 μm).

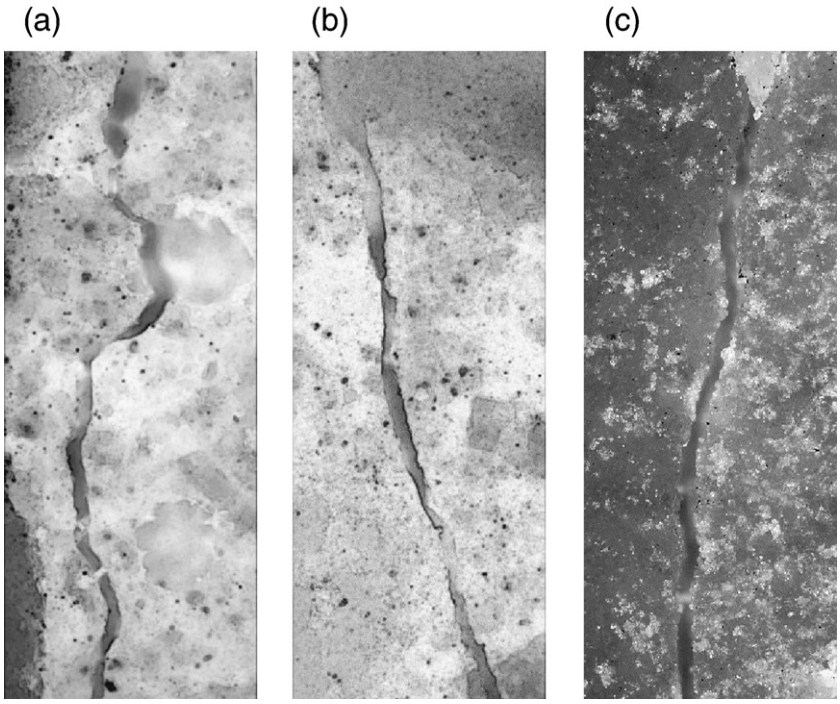

Fig. 9. Microscopic mapping on an unloaded specimen (residual crack width ≈30 μm).

temperature is maintained at 20 °C ± 0.5 °C. Thanks to the two vessels filled with the interstitial solution, the concrete disk soaks in the solution during the whole test.

4.2. Electrical scheme

The electrical scheme is presented in Fig. 4.

To complete the circuit with the electrodes, a reference resistance $R_t = 732\ \Omega$ is added in series in order to determine the applied current *i*. The resistance of the uncracked specimen has been evaluated at about 450–500 Ω while the initial resistance of the electrolyte solution is negligible (<5 Ω).

4.3. Assembly of the set-up

After the preconditioning, the specimen is placed on the press and the apparatus installation is finalized according to Fig. 5. The sample is centered on the press and electrical connections are done. Finally, the testing protocol is followed as described in Section 2.

5. Results and discussion

Two tests were performed with a supply at a constant value of direct current (1 and 5 mA). DC supply was chosen because the data acquisition system used for the mechanical tests is based on DC inputs (± 10 V). The test at 5 mA gave a more satisfying "signal/noise" ratio than at 1 mA and was retained for the purpose of the present analysis. Despite the good results of the 5 mA test, a drift of U1 and U2 was observed. This evidence is well-known [28,29] and is attributed to a polarization of the electrodes in DC measurements which can be avoided by using AC supply. Nevertheless, this drift does not affect the determination of the resistance through the specimen as the drifts of U1 and U2 are similar. However, this drift can affect the determination of the electrolyte resistance in DC measurements. Another apparatus (based on AC measurements) was then used in conjunction with DC measurements, before and after the mechanical test, in order to determine the resistivity of the electrolyte. No variation was found over the period of the mechanical test.

For the sake of completeness, a further test using a square wave compatible with our data acquisition system (10 Hz, ±4 V) was performed to check the feasibility of AC measurements. In such a case, the results were in good agreement with the previous values.

All the tests were controlled (see Section 2) with the mean value of the 4 LVDTs but two cycles were added between 0 and 100 μm in order to check the effect of a breathing of the crack on the electrical resistance.

Fig. 6(a) shows the evolution of the COD during the loading. The COD starts increasing just after the peak of load. The electrical resistance does not change before the peak of load and starts to decrease as soon as the peak of load is reached. It is supposed that when the crack initiates, the electrolyte fills the gap instantaneously and the resistance through the crack is the resistance of the ionic

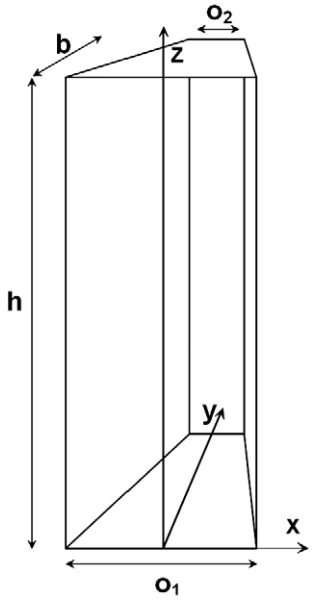

Fig. 10. Crack representation.

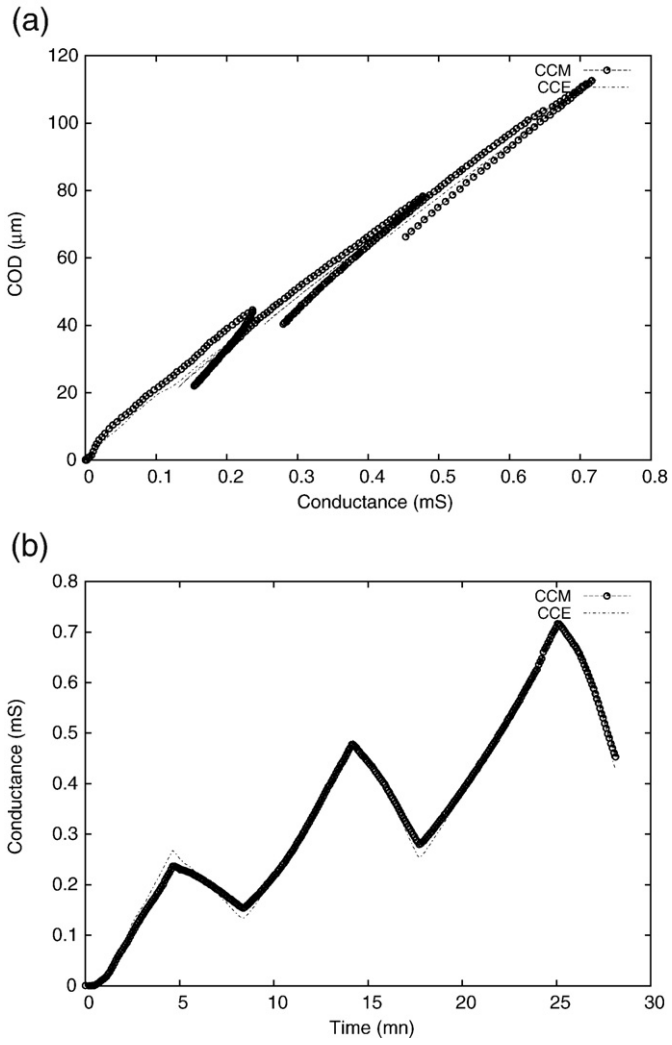

Fig. 11. Model (CCM) and Experimental (CCE) conductances.

solution inside the gap. It can be seen in Fig. 6(b) that the evolution of the overall resistance $((U2-U1)/i)$ follows a path quite similar to the one followed by the COD without threshold effect. During the cycles, the two parameters evolve similarly without any delay between them (see Fig. 6(c)), thus confirming the above hypothesis of the ionic solution filling the crack almost instantaneously. The flow of ionic solution, when the crack is initiated, comes from the vessels and its flow rate is estimated at about 0.5 mm^3/s.

The overall resistance can be defined as above (electrical definition) or as a combination of the resistance of the sound sample and the resistance through the crack. One can consider that this combination can be calculated as two electrical resistances in parallel. The resistance of the sound sample is considered equal to the initial resistance (before the peak). This calculation allows to isolate the resistance through the crack and deduce the crack conductance (CCE) determined by electrical measurements.

As conductance depends on the geometry of the conductor, the crack conductance could possibly be determined with geometrical considerations and assuming a constant value for the conductivity of the ionic solution through the crack. A simple model (CCM) is then proposed in order to identify the key parameters describing the evolution of the conductance depending on the COD.

Firstly, it has been observed that the crack opening mechanism is asymmetrical. The COD measurements via the LVDTs prove to be effective as this measuring system allows to evaluate the crack width on both sides of the specimen. It is important to underline that the visible real crack is tortuous. This crack can be modeled as a succession of parallelograms (Fig. 7(a)) whose surfaces depend only on the local COD and elementary heights, i.e. despite tortuosity, the surface of the modeled crack is almost equivalent to the surface of the real one (Fig. 7(b)). Digital Image Correlation (DIC) observations have highlighted the fact that the COD is almost constant on the crack height except on the zones close to the crack tips (see Fig. 8, full details are given in Ref. [24]). This evidence has also been qualitatively confirmed by microscopic mapping (see Fig. 9). Given the above experimental observations, the global surface has then been modeled via an equivalent rectangular section (neglecting the tips) in which the area is similar to the area of the real crack, though the height is smaller than the real one (as shown in Fig. 7(b)). This height is unknown but can be obtained by fitting. The full crack geometry is then modeled as a truncated prism (see Fig. 10) which allows to take into account all the above considerations.

For what concerns the path tortuosity of the traversing crack, it has been chosen not to include it in the modeling [19].

The electrical resistance, R_c, of the prism is modeled assuming that the sum of the elementary resistances dr_c of slices of thickness dy and area $S(y)=h\times o(y)$ where $o(y)$ is a function giving the width:

$$o(y) = \alpha y + \beta \tag{1}$$

where $\alpha = \frac{o_2 - o_1}{b}$ and $\beta = o_1$, o_1 and o_2 being respectively the front and rear crack openings.

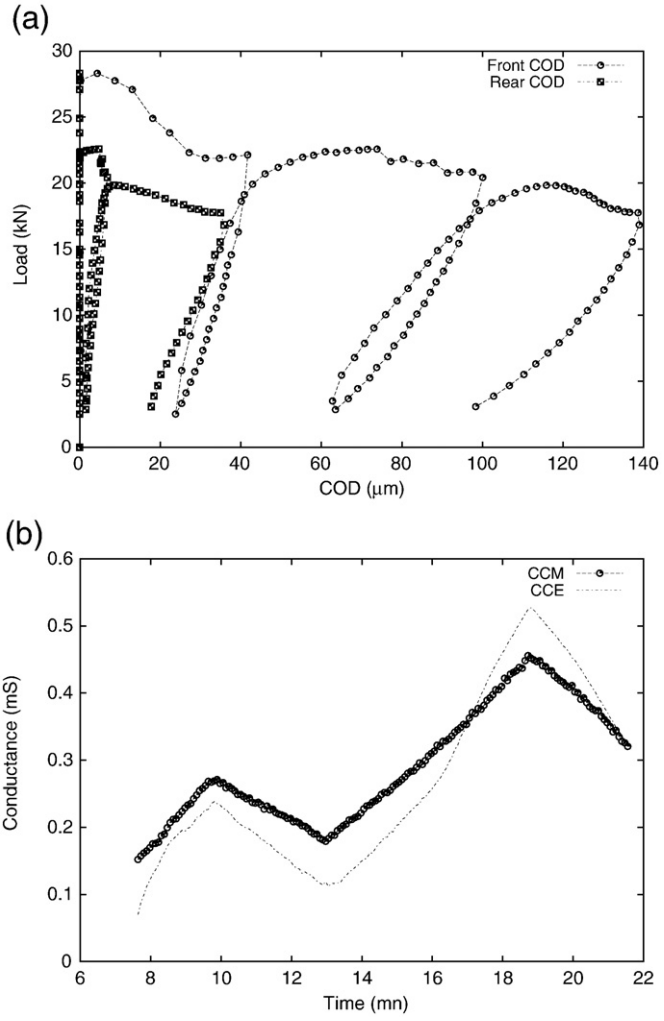

Fig. 12. COD vs. load and Model (CCM)/Experimental (CCE) conductances vs time.

R_c can be then obtained by integrating $dr_c = \rho\frac{dy}{S(y)}$ between 0 and the thickness b:

$$R_c = \frac{\rho}{\alpha h}[\ln(\alpha b + \beta) - \ln(\beta)] \quad (2)$$

The conductance CCM can then be calculated. In this relation α, β and b are known or measured geometrical parameters and the electrolyte resistivity ρ is determined by a measurement of the conductivity, $\sigma = \frac{1}{\rho}$, of the solution at the beginning and at the end of the test (σ=5 S/m). The value of the conductivity is unchanged during the test thanks to the low current intensity. The height, h, of the prism is fitted by minimizing the difference between CCM and CCE. These values are shown in Fig. 11(a) and (b), with a fitted value of h equals to 0.066 m. Such a value seems realistic given the sample dimensions and the hypothesis made on the crack shape.

This h adjustment is sufficient to show that this simple model is in good agreement with experimental observations. Moreover a linear relation exists between the mean crack opening displacement and the electrolyte conductance through the crack (slope = 6.24 ms/μm). This model is based on the hypothesis of a traversing crack, i.e. the transition when the crack starts from one face and propagates to the other, is not taken into account. These observations seem to indicate that the tortuosity of the crack path is not a key parameter controlling crack conductance: this observation is in accordance with Ref. [19]. In the case of a coarser dissymmetry (see Fig. 12(a)), another test showed, nevertheless, a good behavior of the model (see Fig. 12(b)) with similar slope and crack height (h = 0.069 m, slope = 5.15 mS/μm).

6. Conclusion

In order to perform transfer properties tests on cracked concretes under loading, a displacement controlled splitting test has been designed. This test gives crack openings derived from diameter variations measured via LVDTs at mid height of the cylindrical sample. Electrical measurements were then performed in order to monitor the evolution of the electrical resistance of samples, saturated with a basic solution, before and after the peak of load. These measurements were taken in real time so that parasite effects can be minimized. It has been observed that the electrical resistance is constant before the peak and decreases just when the peak of load is reached and when a crack is initiated. It means that, as small as it is, the crack is always filled with the ionic solution (through which ions are completely mobiles) for the chosen displacement rate of the test.

A simple model describing the conductance and taking into account the geometrical evolution of the crack is proposed. This model and the electrical determination of the conductance through a traversing crack are in good agreement so the hypothesis of a constant value for the electrolyte conductivity is verified for a crack width up to 100 μm. In this range, the conductance can be considered instantaneously proportional to the mean crack width (about 6 mS/μm) without any delay between the two parameters.

Further practical applications for such a mechanical protocol can be easily extended to standard water/gas permeability tests in order to obtain real-time measurements on a cracking specimen with an extension of the COD above the value of 100 μm and avoiding lateral cracks. The COD measurements will be also extended to surface measurements with a digital image correlation technique [24] as DIC seems a promising tool for the evaluation of the COD all along the path of the crack.

References

[1] P. Acker, C. Boulay, P. Rossi, On the importance of initial stresses in concrete and of the resulting mechanical effects, Cement and Concrete Research (17) (1987) 755–764.
[2] S. Dal Pont, S. Durand, B. Schrefler, A multiphase thermo-hydro-mechanical model for concrete at high temperatures. Finite element implementation and validation under LOCA load, Nuclear Engineering and Design 237 (22) (2007) 2137–2150.
[3] M. Saito, H. Ishimori, Chloride permeability of concrete under static and repeated compressive loading, Cement and Concrete Research 4 (25) (1995) 803–808.
[4] K. Wang, C. Daniel, S. Jansen, P. Shah, A. Karr, Permeability study of cracked concrete, Cement and Concrete Research 3 (27) (1995) 381–393.
[5] A. Djerbi, S. Bonnet, A. Khelidj, V. Baroghel-Bouny, Influence of traversing crack on chloride diffusion into concrete, Cement and Concrete Research 38 (2008) 877–883.
[6] M. Lepech, C. Victor, Water Permeability of Cracked Cementitious Composites", ICF11, Turin, Italy, 2005.
[7] J. Charron, E. Denarié, E. Bruehwiler, Permeability of ultra high performance fiber reinforced concretes (UHPFRC) under high stresses, Materials and structures 40 (2007) 269–277.
[8] C. Aldea, S. Shah, A. Karr, The permeability of cracked concrete, Materials and Structures 32 (1999) 370–376.
[9] O. Rodriguez, R. Hooton, Influence of cracks on chloride ingress into concrete, ACI Materials Journal March–April, 2003, pp. 120–126.
[10] M. Hardy, J. Hudson, C. Fairhurst, The failure of rock beams. Part 1: theoretical studies, International Journal of Rock Mechanics and Mining Sciences 10 (1973) 53–67.
[11] M. Hardy, J. Hudson, C. Fairhurst, The failure of rock beams. Part 1: experimental studies, International Journal of Rock Mechanics and Mining Sciences 10 (1973) 69–82.
[12] H. Simon, G. Nahas, N. Coulon, Air-steam leakage through cracks in concrete walls, Nuclear Engineering and Design 237 (15–17) (2007) 1786–1794.
[13] C. Andrade, Calculation of initiation and propagation periods of service life of reinforcements by using the electrical resistivity, RILEM Symposium on Concrete Science and Engineering: A Tribute to Arnon Bentur, 2004.
[14] V. Baroghel-Bouny, Which toolkit for durability evaluation as regards chloride ingress into concrete? Part II: development of a performance approach based on durability indicators and monitoring parameters, 3rd Int. RILEM Workshop: Testing and Modelling Chloride Ingress into Concrete, 2002, pp. 137–163.
[15] V. Baroghel-Bouny, Durability indictors: a basic tool for performance-based evaluation and prediction of RC durability, Seminar on Durability and Life-cycle Evaluation of Concrete Structures, Hiroshima, Japan, 2004, pp. 13–22.
[16] V. Baroghel-Bouny, Nouvelle approche de la durabilité du béton. Indicateurs et méthodes, Techniques de l'ingenieur, 2005.
[17] E. 12390-6, Testing hardened concrete—Part 6: Tensile Splitting Strength of Test Specimens, 2001.
[18] J. Torrenti, P. Acker, C. Boulay, D. Lejeune, Contraintes initiales dans le béton, BLPC 158 (1988) 39–44.
[19] M. Ismail, A. Tourni, R. Francois, R. Gagne, Effect of crack opening on the local diffusion of chloride in cracked mortar samples, Cement and Concrete Research 38 (2008) 1106–1111.
[20] J. Réthoré, A. Gravouil, F. Morestin, A. Combescure, Estimation of mixed mode stress intensity factors using digital image correlation and an interaction integral, International Journal of Fracture 132 (2005) 65–79.
[21] F. Hild, S. Roux, Digital image correlation: from displacement measurement to identification of elastic properties—a review, Strain 42 (2006) 69–80.
[22] M. Sutton, S. McNeill, J. Helm, Y. Chao, Advances in two-dimensional and three-dimensional computer vision, Photomechanics (2007) 323–372.
[23] S. Roux, F. Hild, S. Pagano, A stress scale in full-field identification procedures: a diffuse stress gauge, European Journal of Mechanics—A/Solids 24 (3) (2005) 442–451.
[24] C. Boulay, S. Dal Pont, A. Delaplace, H. Delahousse, J.-L. Tailhan, An Experimental Test for Cracking Concrete Under Controlled Conditions, , 2009 ICF12.
[25] C. Sirieix, J. Lataste, D. Breisse, M. Frappa, Caractérisation de l'endommagement du béton par mesures électriques, Materials and structures 35 (2002) 204–210.
[26] J. Torrenti, O. Didry, J. Ollivier, F. Plas, La dégradation des bétons, Hermes, 1999.
[27] M. Thierry, Modélisation de la carbonatation atmosphérique des bétons—prise en compte des effets cinétiques et de l'évolution de la microstructure et de l'état hydrique, Ph.D. thesis, ENPC,Paris (2005).
[28] N. A05-252, Aciers galvanisés ou non au contact de matériaux naturels de remblai, 1990.
[29] J. Ollivier, J. Marchand, L. Nilsson, Méthodologie de prévision de la pénetration des ions chlore par diffusion dans le béton, Béton, du matériau á la structure, RILEM, 1996.